

Model-based design of experiments for adsorption isotherms

Matthias Henninger 10 · Patrik Postweiler 10 · Mirko Engelpracht 10 · Federico Galvanin 20 · André Bardow 30

Received: 28 May 2025 / Revised: 17 August 2025 / Accepted: 12 September 2025 © The Author(s) 2025

Abstract

Designing adsorption processes requires knowledge of the adsorption isotherms. Measuring accurate isotherms is time consuming and inefficient equidistant points are usually chosen. Here, we combine isotherm measurements with Model-Based Design of Experiments to iteratively determine isotherm models with less experimental effort, while maintaining high model accuracy. Our joint approach combining isotherm model discrimination and parameter precision is validated by thermo-gravimetric experiments for the adsorption pairs Lewatit VP OC 1065 with CO₂ and H₂O and BAM-P109 with H₂O, covering isotherm Types I, III, and V. Results show that the experimental effort could be reduced between 70–81%. Furthermore, the framework scheduled measurements for Lewatit VP OC 1065/H₂O to discriminate its isotherm Type between II or III, devoid of our bias as experimenters. Overall, our approach demonstrates potential to streamline the identification of adsorption isotherms while enabling more efficient and unbiased model development.

Keywords Lewatit VP OC 1065 \cdot BAM-P109 \cdot CO $_2$ \cdot H $_2$ O \cdot Magnetic suspension balance measurements \cdot Experimental validation \cdot Parameter estimation

			•
Λh	hra	<i>/// 31</i>	ions
ΛU	ישוטו	viai	IUIIS

BAM	German Institute for Material Science
BET	Brunauer-Emmett-Teller
CV	Coefficient of Variation
DA	Dubinin-Astakhov
GUM	Guide to the expression of uncertainty in
	measurement
HR	Hunter-Reiner
IUPAC	International Union of Pure and Applied
	Chemistry
JCGM	Joint Committee for Guides in Metrology
LTT	Institute of Technical Thermodynamics

Federico Galvanin f.galvanin@ucl.ac.uk

Published online: 26 October 2025

- André Bardow abardow@ethz.ch
- Institute of Technical Thermodynamics (LTT), RWTH Aachen University, Aachen 52062, Germany
- Department of Chemical Engineering, UC London, WC1E 7JE London, UK

(RWTH Aachen)

³ Energy & Process Systems Engineering (EPSE), Department MAVT, ETH Zürich, 8092 Zurich, Switzerland

MBDoE	Model-Based Design of Experiments
MBDoAE	Model-Based Design of Adsorption

Experiments

NIST National Institute of Standards and

Technology

Latin Symbols

- A Adsorption potential $J kg^{-1}$
- b Affinity constant Pa^{-1}
- C BET parameter –
- **D** Design space –
- E Activation energy $\operatorname{J}\operatorname{mol}^{-1}$
- g BET parameter –
- M Molar mass kg mol⁻¹
- m Mass kg
- *n* Isotherm exponent parameter –
- *n* Number –
- P Power W
- p Pressure Pa
- Q Sensitivity matrix –
- R Ideal gas constant $\operatorname{J}\operatorname{mol}^{-1}\operatorname{K}^{-1}$
- T Temperature K
- t_i Student's t-values —
- u Standard uncertainty –
- u Model input vector –



103 Page 2 of 17 Adsorption (2025) 31:103

V Covariance matrix –

 V_0 Prior information matrix –

X Mass-specific loading kg kg⁻¹

x Model variable vector –

y Model response vector –

 \hat{y} Estimated model response vector –

Greek Symbols

 α Significance level –

 Δ Difference –

 ϵ Measurement error vector –

 θ Parameter vector –

 $\hat{\boldsymbol{\theta}}$ Estimated parameter vector –

 σ Standard deviation vector –

 φ Measurement point vector –

 φ^* Optimal measurement point vector –

 χ Chi-value –

 ψ Design criterion –

Subscripts

sat

sor

Equilibrium eq exp Experiment fit Fitted G G-criterion HR HR-criterion Maximal max min Minimal Relative rel

Saturation

Adsorbent

1 Introduction

Adsorption isotherm measurements form the basis for designing adsorption systems in both process and thermal engineering. The magnetic suspension balance is the most accurate sorption measurement technique [1]; however, measuring adsorption equilibrium is slow [2] making experiments costly and time consuming.

To design an adsorption system, isotherm models are fitted to the isotherm measurements. However, not all measurement points of an isotherm measurement contribute equally to identifying the isotherm model parameters. For example, the measurement points close to the inflection point of a Type V isotherm contain much more information for the isotherm model than most of the measurement points in the pressure-insensitive regions away from the inflection point. Knowing the most meaningful measurement points of a given adsorption pair a-priori is no easy task.

The identification of the most informative measurements is the goal of Model-Based Design of

Experiments (MBDoE) [3]. MBDoE is a Design of Experiment approach that optimizes the experimental conditions leveraging the mechanistic model of a process. MBDoE aims to identify and select only the high information points of a given data set [3]. To identify this information content, objective functions are optimized depending on the study goal: E.g., the objective function could discriminate between rivaling models, or could increase parameter precision of the model parameters [3]. Usually, an adequate model is determined first, and model parameters are estimated subsequently. Optimal experimental design for model discrimination and parameter precision can also be alternated [3] or be carried out simultaneously [4].

Although MBDoE approaches have been investigated since the 1950s [5] and research on adsorption is also established itself, the two research areas have rarely been combined. The following chronological literature overview summarizes advances that have been made while applying MBDoE to adsorption measurements and models.

The basics for applying MBDoE to adsorption were laid by Atkinson et al. [6], who applied D-optimal designs for parameter estimation to consecutive and reversible chemical reactions. They also provided optimal designs for model discrimination to determine the reaction order and proposed statistical hypothesis testing to verify the result. Rodríguez-Aragón et al. [7] applied c- and D-optimal design for parameter estimation of the Arrhenius equation, which forms the basis for describing many physical and chemical processes that involve an activation energy (e.g., adsorption).

Later, Rodríguez-Aragón et al. [8] analyzed a number of isotherm models from liquid-solid adsorption literature and calculated D-optimal designs based on the parametrized isotherms. This retrospective study was aimed to help future researchers investigating the same adsorption isotherm models with fewer measurement points. An expression for the D-optimal design of the 2-parameter BET isotherm and a numerical procedure for the Guggenheim-Andersonde Boer (GAB) isotherm were presented. Model discrimination was considered using a sequential approach before parameter estimation. The numerical procedure for experimental design was later expanded to Freundlich and Langmuir isotherms by Mannarswamy et al. [9].

Munson-McGee et al. [10] designed experiments to discriminate between BET and GAB isotherms with three sets of isotherm parameters each, leading to $2^3 = 8$ isotherm model combinations. Their study was again retrospective where the model parameters were already known and the isotherm models were chosen *a-priori*. Later, Munson-McGee et al. [11] applied D-optimal design to sorption kinetic experiments based on Fick's law of diffusion coupled with an external convective mass transfer coefficient. The study was conducted theoretically for an infinite plane



Adsorption (2025) 31:103 Page 3 of 17 103

of adsorbent with finite thickness, and no experiments were performed. The methodology was expanded to infinite cylinders [12] and compared to spherical geometries [13].

Paquet-Durand et al. [14] investigated optimal experimental design for parameter estimation of water <u>absorption</u> kinetics for the Peleg model. The optimal experimental design was compared to equidistant measurements on a scalar and logarithmic scale. The parameter estimation error could be reduced by 62% compared to the equidistant measurements. Kalyanaraman et al. [15] took measurement data of the MOF adsorption pair CO₂/UiO-66 from the National Institute of Standards and Technology (NIST) database and performed Bayesian design to determine the Langmuir model parameters for this adsorption pair retrospectively. The authors note that "studies on the application of Bayesian design to physical experiments (...) are still scarce".

Kober et al. [16] summarized the results of [8] and [9]. They noted that the liquid solution equilibrium concentration should not be the independent variable of the MBDoE for liquid-solid adsorption since it is a response variable of the system. The authors compared retrospective D-optimal designs for various isotherm models and found optimal experimental designs which depended on all model parameters instead of only a few. The study was expanded by Kober at al. [17] by keeping the initial concentration at its maximal value and varying the ratio between solution volume and adsorbent mass, resulting in better parameter estimates.

Postweiler et al. [18] applied optimal experimental design to validate dynamic adsorption chiller models against measurement data. The experimental design was performed iteratively to reduce uncertainty of unknown parameters in the dynamic model. The authors show their method to lead to a valid adsorption chiller model by executing three dynamic adsorption chiller measurements, thereby reducing experimental effort by 83% compared to random experiments.

Ward and Pini [19] determined the parameter uncertainties of a 1D dynamic column breakthrough model for CO_2 /He adsorption onto activated carbon with Bayesian inference. The authors propagated the parameter uncertainties through the dynamic models to assess their robustness. The results showed that 70% of the dynamic model variability could be attributed to the uncertainty of temperature-dependent isotherm parameters, highlighting the need for exact adsorption isotherm models.

Toffoli de Oliveira et al. [20] optimized parameter estimation of an adsorption breakthrough curve model by employing a Bayesian technique. The operational conditions of volumetric flow, adsorbent mass, and initial adsorptive concentration were varied for caffeine adsorption onto activated carbon. The results proved the Bayesian approach effective, so that all operational conditions obtained a caffeine removal of 95%.

The literature overview shows first applications of MBDoE methods to adsorption experiments, mostly focused on liquid-solid adsorption and retrospective analyses, while application to physical experiments is still scarce. Some studies have been conducted for parameter estimation of breakthrough column models, concluding that the highest uncertainty in the dynamic models can be attributed to the model parameters of the equilibrium isotherm [19]. However, the strength of MBDoE approaches to reduce the actual experimental effort has not been exploited for adsorption isotherms, yet.

In this work, we present a comprehensive method to estimate isotherm parameters and discriminate between rivaling isotherm models when *a-priori* knowledge of the adsorption pair is missing or it would be beneficial to avoid time-consuming equidistant adsorption isotherm measurements. For this purpose, we combine a theoretical framework with adsorption isotherm measurements while focusing on the isotherm model performance rather than individual parameter uncertainty. In Sect. 2, we introduce the experimental setup and reference measurements. In Sect. 3, we present the MBDoE framework and in Sect. 4 we show the results for optimally designed Type I, III, and V isotherm measurements together with a sensitivity analysis of the stopping criterion used in the MBDoE framework. Finally, we conclude our main findings.

2 Experimental setup and reference measurements

2.1 Magnetic suspension balance

A magnetic suspension balance decouples a micro scale and a measurement cell through a magnetic suspension coupling, which levitates a sample basket in a magnetic field [2]. The concept of magnetic suspension balances is based on Gast [21], while modern systems mostly follow the design by Lösch et al. [22]. By moving the scale outside of the measurement cell, a common scale can be used since it is only exposed to benign conditions at ambient pressure and temperature. Meanwhile, pressure and temperature within the measuring cell range from 2×10^{-6} bar to 150 bar and -40° C to 400° C for the gravimetric system (Rubo-SORP 150), which was used for this study. The resolution of the scale is 1 µg (Sartorius MSA66S-000-DH). A custombuilt and automated gas-dosing station ensures the supply of gas or vapor at the desired pressure and temperature. A trace heating system with variable setpoint allows for measurements with condensable vapor without superheating the vapor too much. Furthermore, the gas dosing station is equipped to handle sub-atmospheric pressure as well as



103 Page 4 of 17 Adsorption (2025) 31:103

high pressure allowing for high variability of the selectable adsorbate. A photo of the magnetic suspension balance setup in the laboratory is shown in Fig. 1.

Figure 2 gives a more detailed schematic overview of the main components of the magnetic suspension balance. The description of Fig. 2 follows the work by Dresp [23]: The top of the figure shows an electromagnet attached to the micro scale and a permanent magnet attached to the basket with a suspension rod, forming the magnetic coupling. The position of the basket is detected by a displacement sensor consisting of a sensor core attached to the suspension rod and a sensor coil attached to the wall of the pressure vessel. As a consequence, the position is continually monitored, can be adjusted by feedback control of a PID controller, and can be set by changing the voltage of the electromagnet. With this setup, the magnetic suspension balance transmits the forces on the sample to the micro scale. The "tare" functionality of a balance is realized by a mechanical coupling, allowing to weigh a zero point signal. The zero point signal is subtracted from the measurement signal to receive the actual change in mass of the sample. A sinker with calibrated mass and volume (titanium cylinder) allows to deduce the density of the surrounding adsorptive.

This experimental setup allows to measure the change in mass of an adsorption sample with varying pressure p at a given temperature T. Combined with the dry

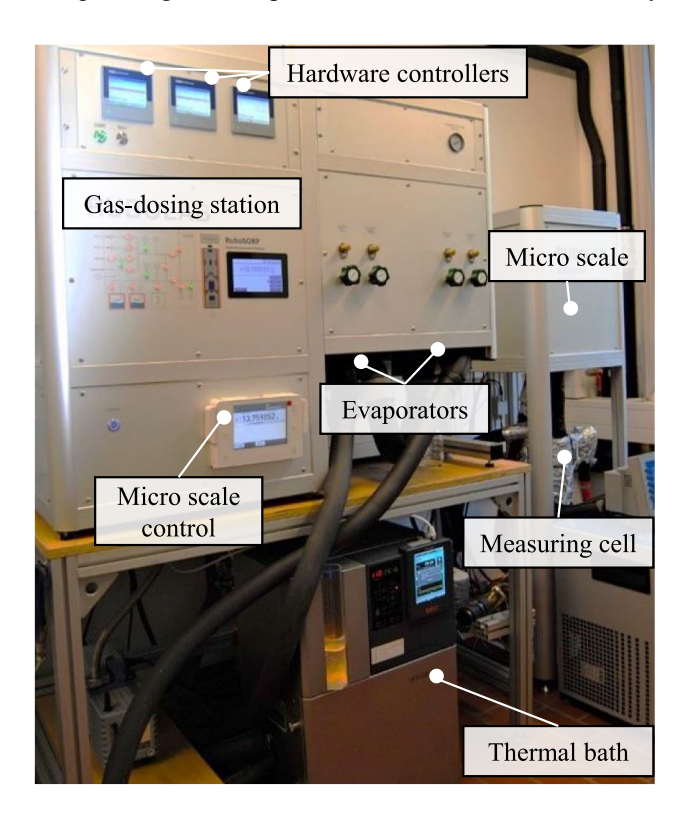
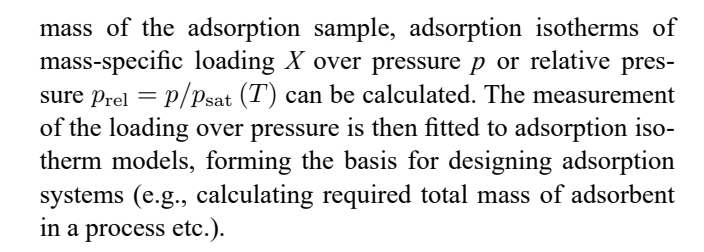


Fig. 1 Photo of the magnetic suspension balance in the lab, including gas dosing station, hardware controllers, evaporators, micro scale and micro scale control, thermal bath, and measuring cell



2.2 Adsorption isotherm models

Taking into account the isotherm types of Lewatit VP OC 1065 with $\rm H_2O$ and $\rm CO_2$ as well as BAM-P109/ $\rm H_2O$, we consider the following isotherm models for this study:

1. The Sips isotherm [24] with 3 parameters X_{eq} , b, and n, which can take the form of Type I, III, and V isotherms:

$$X(p_{\rm rel}) = X_{\rm eq} \frac{(b \, p_{\rm rel})^{1/n}}{1 + (b \, p_{\rm rel})^{1/n}}.$$
 (1)

2. The adjusted BET-isotherm [25] with 4 parameters $X_{\rm eq}$, C, g, and n, which can take the form of all isotherm types except Type VI:

$$X(p_{\text{rel}}) = X_{\text{eq}} \frac{C p_{\text{rel}}}{1 - p_{\text{rel}}} \frac{1 + n \left(\frac{g}{2} - 1\right) p_{\text{rel}}^{n-1} - (n g - n + 1) p_{\text{rel}}^{n} + \frac{g}{2} n p_{\text{rel}}^{n+1}}{1 + (C - 1) p_{\text{rel}} + C \left(\frac{g}{2} - 1\right) p_{\text{rel}}^{n} - \frac{g}{2} C p_{\text{rel}}^{n+1}}.$$
(2)

3. The Dubinin-Astakhov (DA) isotherm [26] with three parameters $X_{\rm eq}$, E and n, which can take the form of Type I, II, III, and V isotherms

$$X(p_{\rm rel}, T) = X_{\rm eq} e^{-\left(\frac{A}{E}\right)^n}, \tag{3}$$

with the adsorption potential A given by:

$$A(p_{\rm rel}, T) = \frac{R}{M} T \log \left(\frac{1}{p_{\rm rel}}\right). \tag{4}$$

In practice, an isotherm model needs to describe the adsorption behavior at varying temperatures [27]. Temperature dependencies have taken different forms and sometimes vary even within the same isotherm model [28]. Also, it is discussed whether all parameters should be dependent on temperature [28]. Here, we employ temperature dependence of the parameters as described for the Sips model [27]:

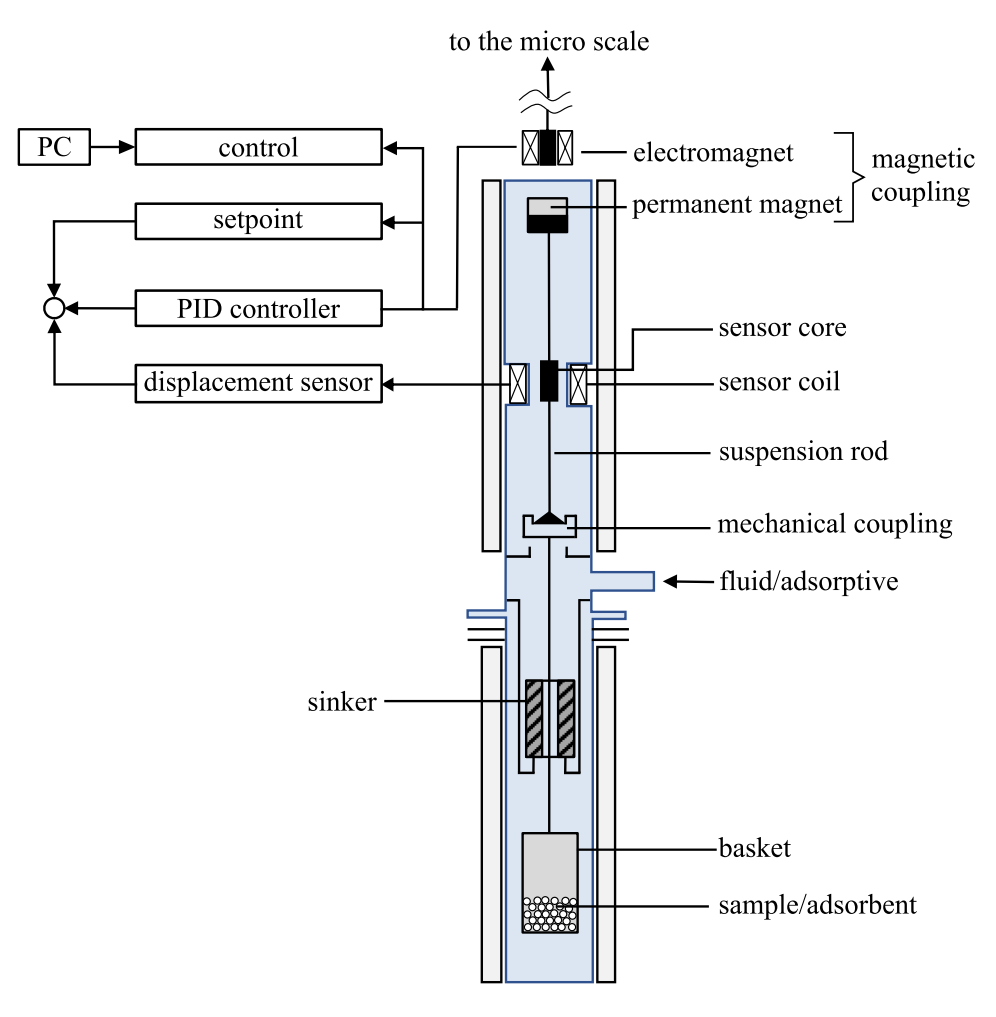
$$X_{\rm eq} = X_0 e^{X_T \left(1 - \frac{T}{T_{\rm ref}}\right)}, \tag{5}$$

$$b = b_0 e^{b_T \left(\frac{T_{\text{ref}}}{T} - 1\right)}$$
, and (6)



Adsorption (2025) 31:103 Page 5 of 17 103

Fig. 2 Schematic of the magnetic suspension balance redrawn after Rother et al. [1]



$$\frac{1}{n} = \frac{1}{n_0} + n_T \left(1 - \frac{T_{\text{ref}}}{T} \right)$$
 (7) 2.3.1 χ^2 -test

All equations incorporate an arbitrary reference temperature $T_{\rm ref}$ where the temperature dependencies reduce to the factor one. While the temperature dependence of the parameter b is taken from the Langmuir equation, the temperature dependence of the parameter n is empirical. The temperature dependence of the parameter $X_{\rm eq}$ is also empirical and sometimes even neglected [27].

2.3 Statistical analyses of the experiments

When comparing isotherm measurements to isotherm models, a set of statistical hypothesis tests helps evaluating the validity of the model identification results [29]. The two tests are the χ^2 -test and Student's t-test, which are presented following Pankajakshan et al. [29].

The chi-square (χ^2) goodness of fit test can be applied to every isotherm model to test if the hypothesis of randomly distributed measurement errors can be confirmed or rejected. This hypothesis test is performed by evaluating the residuals between outputs \boldsymbol{y} (e.g., measurements) and isotherm model predictions $\hat{\boldsymbol{y}}$. The χ^2 -test evaluates whether the residuals can be considered as a random sample of a specified normal error distribution or if there is a systematic deviation, meaning the model does not match the data. The χ^2 -test characteristic is calculated according to

$$\chi^{2} = \frac{1}{\sigma_{\boldsymbol{y}}^{2}} \sum_{i=1}^{n_{\boldsymbol{y}}} \left[y_{i} - \hat{y}_{i} \left(\boldsymbol{\theta} \right) \right]^{T} \left[y_{i} - \hat{y}_{i} \left(\boldsymbol{\theta} \right) \right], \qquad (8)$$

with the standard deviation of the outputs σ_y and the model parameters θ . The model parameters of the isotherm models are $\theta_{\mathrm{Sips}} = \{X_0, X_T, b_0, b_T, n_0, n_T\}$, $\theta_{\mathrm{BET}} = \{X_0, X_T, g_0, g_T, n_0, n_\theta\}$ (a) $\mathcal{L}\{X_0, X_T, E_0, E_T, n_0\}$ (i) Eqs. (1) to (7)). The χ^2 value is compared to a reference χ^2 value $\chi^2_{\mathrm{ref}} = \chi^2_{n_y - n_\theta} (1 - \alpha)$. This reference value χ^2_{ref} is



taken from a χ^2 distribution with n_y-n_θ degrees of freedom, where n_y represents the number of measurements and n_θ the number of parameters of a model. The significance level α defines the point at which the test is deemed successful: For a high significance level, models with high residuals will be accepted sooner while a low significance level might lead to none of the models meeting the required accuracy. A common significance level is 5% implying a remaining probability of 5% that the hypothesis of the residuals matching a normal error distribution is falsely confirmed and the associated isotherm model should actually be rejected.

The χ^2 -test can also be inverted to check for the probability of each model which would satisfy the hypothesis of the model's residuals following a normal distribution. The test then returns an α -level which is also called p-value.

If multiple models pass the χ^2 -test, assigning a probability to each model becomes useful. Here, we use the equivalent probability \Pr_i from Pankajakshan et al. [29]

$$\Pr_{i} = \frac{\Pr\left(\chi_{i}^{2} \leq \chi_{n_{y}-n_{\theta}}^{2}\right)}{\sum_{i=1}^{n_{\text{models}}} \Pr\left(\chi_{i}^{2} \leq \chi_{n_{y}-n_{\theta}}^{2}\right)} \qquad \forall i = 1, \dots, n_{\text{models}},$$

$$(9)$$

where the probability Pr() is equal to the p-value from the χ^2 -test for the *i*-th model. The larger the probability, the more residuals are not contradicted by the distribution of measurement error [29].

Related to the χ^2 value is the Coefficient of Variation (CV) (i.e., the relative standard deviation):

$$CV = \frac{\sqrt{\frac{1}{n_y} \sum_{i=1}^{n_y} (y_i - \hat{y}_i(\boldsymbol{\theta}))^2}}{\frac{1}{n_y} \sum_{i=1}^{n_y} y_i} \qquad \forall i = 1, ..., n_y.$$
 (10)

The coefficient of variation relates the root mean square deviation to the mean of the measurements. The CV is often given in percent: A CV value of 0% indicates a perfect fit of the model to data, while a CV of 100% indicates a root mean square deviation equal to the mean value of the measurements. The CV value quantifies the overall predictive accuracy of the fitted models and allows for direct comparison between rivaling models.

2.3.2 Student's t-test

The Student's t-test is performed to assess the precision of the model parameters. The goal of the t-test is to confirm whether the variation of the parameters can be explained from the variation of the data. A variation of the parameter estimates can be taken directly from the parameter covariance matrix V_{θ}



with the sensitivity matrix Q according to

$$Q = \begin{bmatrix} \frac{\partial \hat{y}_1}{\partial \theta_1} & \cdots & \frac{\partial \hat{y}_1}{\partial \theta_{n_{\text{parameter}}}} \\ \cdots & \cdots & \cdots \\ \frac{\partial \hat{y}_{n_{\text{outputs}}}}{\partial \theta_1} & \cdots & \frac{\partial \hat{y}_{n_{\text{outputs}}}}{\partial \theta_{n_{\text{parameter}}}} \end{bmatrix},$$
(12)

and the standard deviation of the outputs (i.e., of the measurements) σ_y . In case there are prior information on the parameters (e.g., from parameter bounds or the first curve fit), the prior information matrix $V_{\theta,0}$ is added.

From the main diagonal of the covariance matrix $(V_{\theta,ii})$, the test statistic (t-values t_i) from Student's t-test can be calculated according to

$$t_{i} = \frac{\hat{\theta}_{i}}{t_{n_{\boldsymbol{y}} - n_{\boldsymbol{\theta}}} \left(1 - \alpha/2\right) \sqrt{V_{\boldsymbol{\theta}, ii}}} \qquad \forall i = 1, ..., n_{\boldsymbol{\theta}}, \qquad (13)$$

where $\hat{\theta}_i$ are estimates of the individual parameters and α is the significance level. The computed t-values are then compared to reference t-values from Student's t-distribution $t_{n_{\pmb{y}}-n_{\pmb{\theta}}}$ $(1-\alpha/2)$. The reference t-value is taken from a two-tailed t-distribution with $n_{\pmb{y}}-n_{\pmb{\theta}}$ degrees of freedom, where $n_{\pmb{y}}$ is the number of measurements and $n_{\pmb{\theta}}$ the number of parameters of the model. Parameters with t-values larger than the reference t-value are considered well estimated [29].

2.4 Reference isotherm measurements

Reference measurements are needed to evaluate the resulting experimental designs of the MBDoE framework. To test our design approach for a broad range of applications, our measurements encompass the three isotherm Types I, III, and V, and use adsorption pairs with high relevance in the field of adsorption: Lewatit VP OC 1065 with CO₂ (Type I isotherm) and H₂O (Type III isotherm) as well as BAM-P109 with water (Type V isotherm). Lewatit VP OC 1065 is a highly researched amine-functionalized polymer manufactured by Lanxess GmbH, which can directly capture CO₂ from the atmosphere [30]. BAM-P109 is an activated carbon with defined properties provided by the German Institute for Materials (BAM) and was recently employed in an inter-laboratory study by Nguyen et al. from the US National Institute of Standards and Technology (NIST) [31]. The study aimed to provide a water calibration isotherm for new isotherm measurement systems. Gathering data from multiple laboratories enabled statistically significant results. For these three adsorption pairs, we measure equidistant reference isotherms (i.e., evenly



Adsorption (2025) 31:103 Page 7 of 17 103

Fig. 3 Reference measurement of a Type I isotherm with Lewatit VP OC 1065/CO₂ (LTT). The adsorption pair was measured at 25 °C (left), 75 °C (center), and 100 °C (right) and compared to literature data from Young et al. [30]. The three isotherm models DA (dotted), BET (densely dashed), and Sips (dashed) were fitted to the measurement results. An analysis of the measurement uncertainty is given in Appendix A

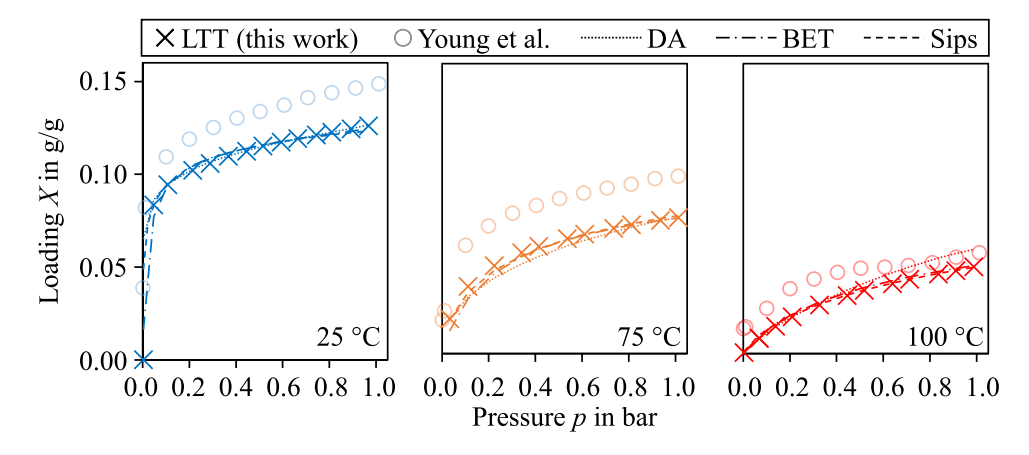


Table 1 Results of the Type I isotherm calibration

Model	X_0	X_T	$(b/E/g)_0$	$(b/E/g)_T$	n_0	n_T	C_0	C_T	CV
Sips	0.170	1.487	18.66	17.01	2.95	1.962	_	_	12.4%
DA	0.127	3.141	500.1	7.736	0.88	-1.251	_	_	17.5%
BET	0.123	−5.5 e-3	0.601	11.19	1.54	_	43.54	16.27	5.4%

The isotherm models yield the loading X in $g g^{-1}$ when inserting the pressure p in bar and the parameters X, b, E, g, n, and C as given. Parameters defining the temperature dependence according to Eqs. (5) to (7) are denoted with the index T while the base parameters are denoted with the index 0. Bold models indicate the chosen reference model with the lowest CV value

spaced sampling over the pressure range) with the commercial gravimetric system from Rubolab from Sect. 2.1. We compare the measurements to literature data and fit the isotherm models of Sips (Eq. (1)), adjusted Brunauer-Emmett-Teller (BET) (Eq. (2)), and Dubinin-Astakhov (DA) (Eq. (3)) to the experiments.

Figure 3 shows the reference isotherms of Lewatit VP OC 1065/CO₂. Our measurements (LTT) follow the trend of the data points from Young et al. [30].

However, we underestimate the absolute loading by an almost constant relative offset between 15-20% for all three temperatures. The difference can be explained by different batches of Lewatit or by the initial desorption (or activation) process of the material: Although the Lewatit sample was desorbed in-situ at the same temperature and for the same duration as in Young et al. [30], we only had access to a rotary vane vacuum pump instead of a turbo-molecular vacuum pump. The turbo-molecular pump in the work from Young et al. [30] desorbed the sample at lower pressure than our rotary vine pump, leading to better desorption. Further desorption leads to a smaller sample mass and in turn to higher loading. The constant relative offset between 15–20% supports this hypothesis (Fig. 3 left and center). The slightly decreasing offset towards high pressure at 100 °C (Fig. 3 right) might be due to the measurement data of Young et al. [30] as the plateau between $p = 0.6 \,\mathrm{bar} - 0.8 \,\mathrm{bar}$ at $100 \,^{\circ}\mathrm{C}$ was neither visible at lower temperatures nor at our data at high temperature. If there was in fact a physical effect happening between $p = 0.6 \,\mathrm{bar} - 0.8 \,\mathrm{bar}$ at 100 °C, it has not been explained.

Despite the differences between our measurement and the literature, the set of isotherms is well suited as a reference measurement for the MBDoE framework as all three isotherm models can be calibrated using the data. Also, the temperature dependence of a Type I isotherm is clearly visible. Results after model calibration are reported in Table 1 including the isotherm with the lowest CV-value $CV_{BET} = 5.4\%$. Sips and DA isotherms have CV-values of $\mathrm{CV_{Sips}} = 12.4\,\%$ and $\mathrm{CV_{DA}} = 17.5\,\%,$ respectively. The probability from the χ^2 -test is almost the same for all three models ranging between 32-34%. The DA model captures the steep gradient at low pressures the best. However, the DA model underestimates the loading at 50 °C and overestimates the loading at 100 °C, which could be improved with different equations for the temperature dependency.

Figure 4 shows the reference isotherm of Lewatit VP OC $1065/\mathrm{H}_2\mathrm{O}$. Our data shows good agreement with the measurement from Young et al. [30]. We were able to measure up to relative pressures of $p_{\mathrm{rel}} < 0.85\,\mathrm{Pa}\,\mathrm{Pa}^{-1}$ as water started to condensate onto the suspension rod, the mechanical coupling and the sinker, preventing accurate measurements beyond $p_{\mathrm{rel}} = 0.85\,\mathrm{Pa}\,\mathrm{Pa}^{-1}$. These parts of the magnetic suspension balance cannot be heated separately, thus limiting the range of relative pressure our setup could cover. The largest deviation of $0.07\,\mathrm{g}\,\mathrm{g}^{-1}$ to Young et al. [30] is at high pressure and 75 °C. This deviation is most likely due to the nature of the adsorption process of the Lewatit polymer: The water leads to swelling of the polymer [32], which increases the pore size, makes more adsorption



103 Page 8 of 17 Adsorption (2025) 31:103

Fig. 4 Reference measurement of a Type III isotherm with Lewatit VP OC $1065/H_2O$ (LTT). The adsorption pair was measured at $25\,^{\circ}C$ (left), $50\,^{\circ}C$ (center), and $75\,^{\circ}C$ (right) and compared to literature data from Young et al. [30]. The three isotherm models DA (dotted), BET (densely dashed), and Sips (dashed) were fitted to the measurement results. An analysis of the measurement uncertainty is given in Appendix A

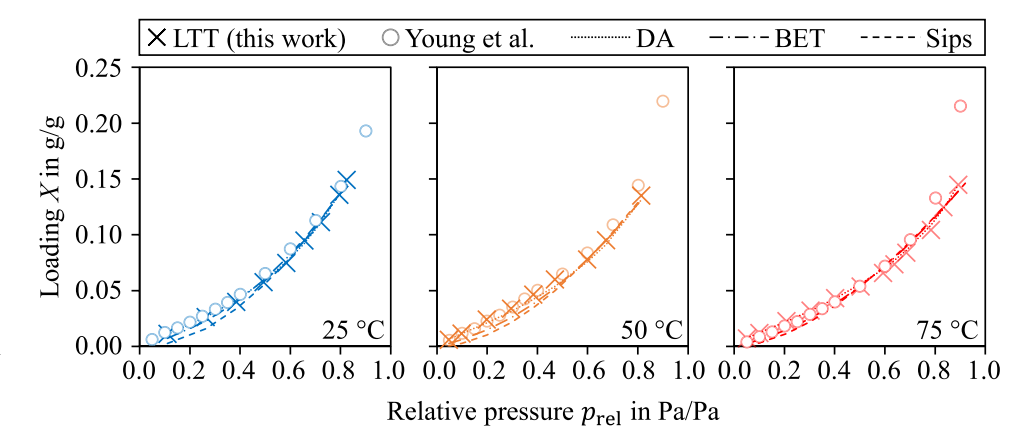


Table 2 Results of the Type III isotherm calibration

Model	X_0	X_T	$(b/E/g)_0$	$(b/E/g)_T$	n_0	n_T	C_0	C_T	CV
Sips	1.909	2.297	0.3501	0.1609	2.01	0.4280	_	_	11.0%
DA	0.338	2.017	37.24	-3.046	0.59	0.0270	_	_	3.6%
BET	0.495	2.406	0.8243	1.370	3.23	_	0.1078	-2.29	7.8%

The isotherm models yield the loading X in g g^{-1} when inserting the relative pressure p_{rel} in Pa Pa⁻¹ and the parameters X, b, E, g, n, and C as given. Parameters defining the temperature dependence according to Eqs. (5) to (7) are denoted with the index T while the base parameters are denoted with the index 0. Bold models indicate the chosen reference model with the lowest CV value

sites available, and leads to the Type III isotherm shape approaching infinite loading. The swelling is very slow. If the kinetics of adsorption are faster than the swelling, points of lower loading will appear equilibrated even though more water could be adsorbed when waiting for the swelling. This effect leads to points of lower loading especially for high relative pressures, because the last points were potentially not equilibrated. Note that, the swelling also affects the buoyancy correction, but since we measure at pressures below 1 bar, the effect of buoyancy itself is negligible and thus also the impact of swelling on the buoyancy.

Overall, the measurements for the Type III isotherm (crosses and circles) resemble the literature data (dash-dotted lines) reasonably well and can be used as reference data for the MBDoE algorithm. The only drawback of this data for a MBDoE study is the low temperature dependency of the adsorption pair, which makes the measurement at multiple temperatures almost superfluous.

Table 2 shows the parameters of all three isotherm models for the Type III isotherm. The DA model fitted the data the best with a coefficient of variation $\mathrm{CV_{DA}} = 3.6\,\%$. All isotherm models provide the same probability from the χ^2 -test and are equally suited to describe the Type III isotherm behavior.

Figure 5 shows the reference isotherm of BAM-P109/ $\rm H_2O$ up to relative pressures of $p_{\rm rel} < 0.85\,\rm PaPa^{-1}$. Our 25 °C isotherm shows good agreement with the interlaboratory study from Nguyen et al. [31]. Here, we provide additional isotherms to Nguyen et al. [31] at 50 °C and 80 °C. The figure shows a slightly decreasing maximum

loading for increasing temperature. Furthermore, the inflection point moved to higher relative pressure. However, as with the Type III isotherm, the temperature dependency is almost negligible.

Table 3 shows the parameters of all three isotherm models for the Type V isotherm with the best fit by the BET model with $\mathrm{CV}_{\mathrm{BET}} = 2.7\,\%$. As with the Type III isotherm, all isotherm models provide the same probability from the χ^2 -test and are equally suited to describe the Type V isotherm behavior.

Overall, 36 data points were measured for the Type I isotherm (Lewatit VP OC $1065/\mathrm{CO}_2$), 30 data points for the Type III isotherm (Lewatit VP OC $1065/\mathrm{H}_2\mathrm{O}$), and 48 data points for the Type V isotherm (BAM-P109/H₂O), and only adsorption was considered. The next section introduces the MBDoE algorithm to reduce this experimental effort, while trying to maintain high-quality isotherm models.

3 MBDoE algorithm and flowchart

The MBDoE algorithm for isotherm measurements follows the general approach by Pankajakshan et al. [29], which is based on Franceschini et al. [3]. The open-source Python code is available in the SI of this study. The mathematical models to be calibrated are generally differential algebraic equation systems (DAE-systems) and can be written as [4]

$$f\left(\frac{\mathrm{d}\boldsymbol{x}\left(t\right)}{\mathrm{d}t},\,\boldsymbol{x}\left(t\right),\,\boldsymbol{u}\left(t\right),\,\boldsymbol{\theta},\,t\right)=0\,,\tag{14}$$



Adsorption (2025) 31:103 Page 9 of 17 103

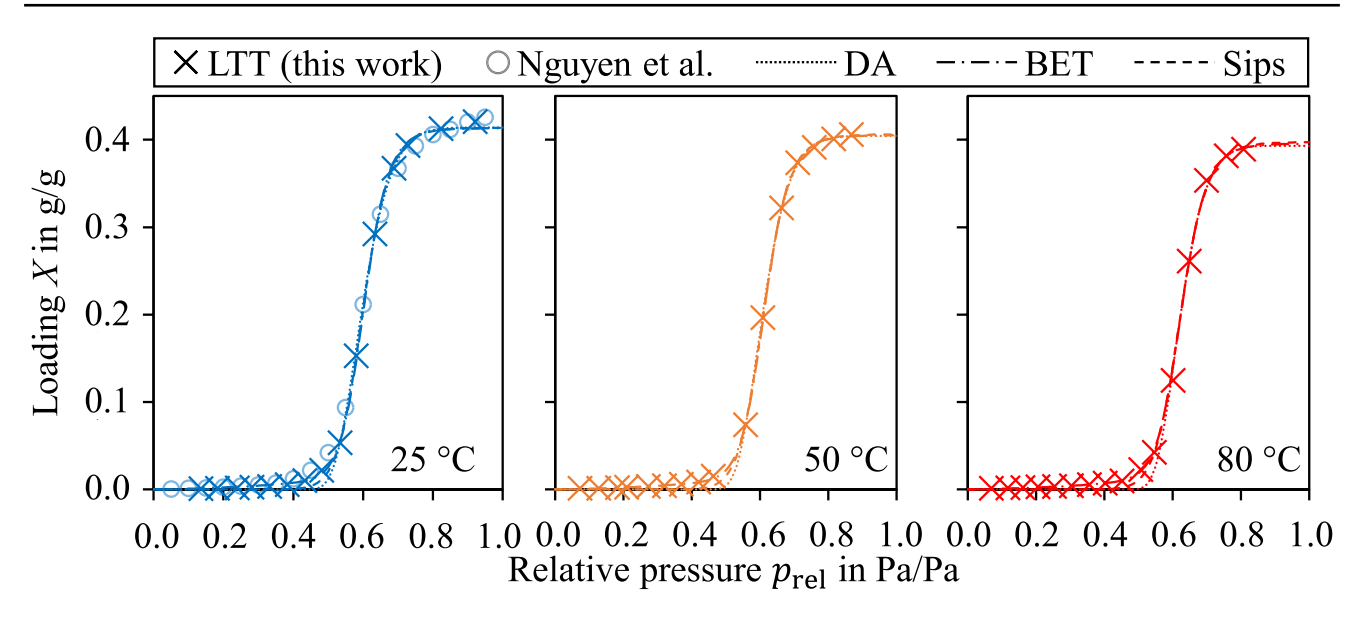


Fig. 5 Reference measurement of a Type V isotherm with BAM-P109/H $_2$ O (LTT). The adsorption pair was measured at 25 $^{\circ}$ C (left), 50 $^{\circ}$ C (center), and 80 $^{\circ}$ C (right) and compared to literature data from Nguyen et al. [31] for 25 $^{\circ}$ C. The three isotherm models DA (dotted),

BET (densely dashed), and Sips (dashed) were fitted to the measurement results. An analysis of the measurement uncertainty is given in Appendix A

Table 3 Results of the Type V isotherm calibration

Model	X_0	X_T	$(b/E/g)_0$	$(b/E/g)_T$	n_0	n_T	C_0	C_T	CV
Sips	0.414	0.220	1.666	0.2342	16.1	-3.6 e-3	_	_	3.8%
DA	0.414	0.280	75.78	-0.537	5.49	−77.8 e-3	_	_	5.2%
BET	0.023	0.237	78.2 e3	3.856	18.2	_	0.364	0.100	2.7%

The isotherm models yield the loading X in g g^{-1} when inserting the relative pressure p_{rel} in Pa Pa⁻¹ and the parameters X, b, E, g, n, and C as given. Parameters defining the temperature dependence according to Eqs. (5) to (7) are denoted with the index T while the base parameters are denoted with the index 0. Bold models indicate the chosen reference model with the lowest CV value

$$\boldsymbol{x}\left(t=0\right) = \boldsymbol{x}_0 \,,\,\text{and} \tag{15}$$

$$g(x(t), u(t), \theta, t) = \hat{y}(t),$$
 (16)

where f represents the differential equations and g the algebraic equations. This general form reduces to Eq. (17) without time dependencies for the isotherm models, since they have no time-dependent variables:

$$g(x, u, \theta) = \hat{y}. \tag{17}$$

The variables x are the algebraic state variables (e.g., pressure p and temperature T in an isotherm model), x_0 are their initial conditions (not needed here), u are the input variables, θ are the model parameters (e.g., $\theta_{\rm Sips}$, $\theta_{\rm BET}$, and $\theta_{\rm DA}$). The output (e.g., loading X in an isotherm model) is represented by y for true outputs (i.e., measurements) and \hat{y} for estimations of the outputs by the models [4]. Likewise, $\hat{\theta}$ denotes estimations of the true model parameters θ . All measurements y_i consist of the true response \hat{y}_i and a measurement error ϵ_i (Eq. (18)). The measurement error ϵ_i consists of a combination of measurement noise and model

lack-of-fit. Here, we assume a measurement error that is independent and identically distributed. We assume other sources of error, such as temperature setting error, degradation of the adsorbent, and insufficient waiting time to reach equilibrium to be insignificant compared to the measurement error of the device.

$$y_i = \hat{y}_i \left(\hat{\boldsymbol{\theta}} \right) + \epsilon_i \,. \tag{18}$$

To generate the next measurement points of the experimental design φ^* (i.e., the next pressure to be measured) in a design space D (i.e., the pressure range), we maximize the information for this next experiment. The information is represented by a design criterion ψ :

$$\varphi^* = \underset{\varphi \text{ in } D}{\operatorname{argmax}} \{\psi\} \ . \tag{19}$$

The design criterion is usually chosen to maximize information either regarding model discrimination or parameter precision. Here, a joint approach is chosen to optimize model



discrimination and parameter precision at the same time. We chose the Hunter-Reiner (HR)-criterion (Eq. (20)) for model discrimination and the G-criterion (Eq. (21)) for parameter precision. The HR-criterion is described by

$$\psi_{\text{HR}} = \sum_{i=1}^{(n_{\text{models}}-1)} \sum_{j=i+1}^{n_{\text{models}}} (\hat{y}_i - \hat{y}_j)^T (\hat{y}_i - \hat{y}_j) , \qquad (20)$$

where \hat{y}_i and \hat{y}_j are predictions of model i and j, respectively, and n_{models} is the total number of considered models. The goal of this design criterion is to find the measurement point where the predictions of all models deviate the most. Alternative criteria for model discrimination have been proposed by Buzzi-Ferraris et al. [33] or Donckels et al. [34] including uncertainty of the measurements or Schwaab et al. [35] using the parameter covariance matrix. Since we assume constant measurement uncertainty and the variance on model prediction was relatively constant, the HR-criterion is regarded as sufficient here and we can neglect normalizing Eq. (20) by measurement errors. However, the provided code base in the supplementary material allows for both variable measurement error and alternative model discrimination criteria.

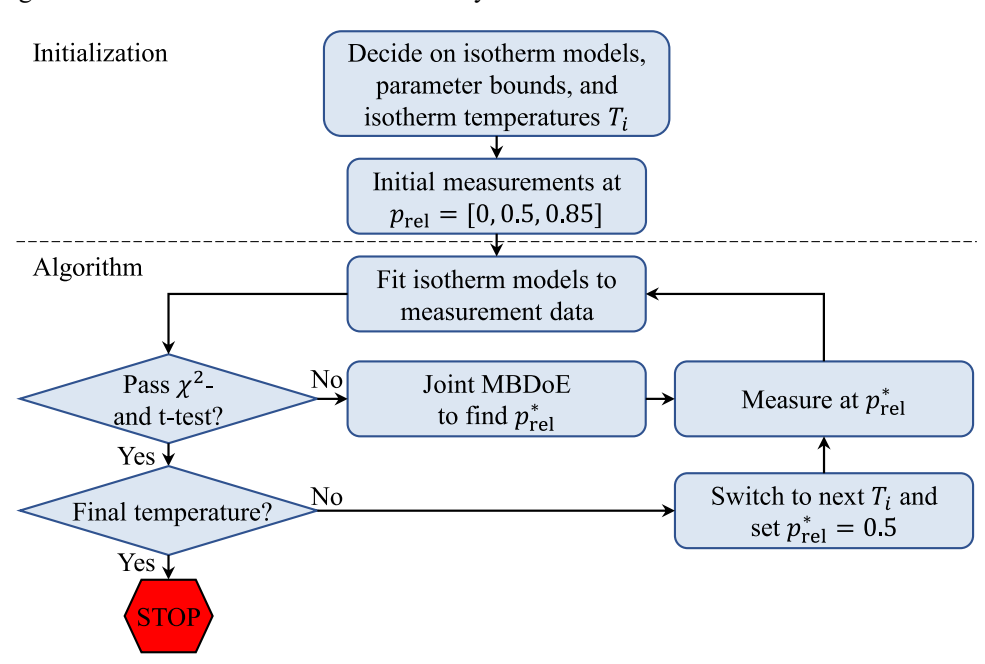
For parameter precision, a scalar value needs to be derived from the parameter covariance matrix V_{θ} (cf. Eq. (11)) to serve as objective function [3]. Various criteria such as A-, D-, and E-optimality are regularly employed. While the A-, D-, and E-criterion aim to minimize the uncertainty of the parameters θ , the G-criterion minimizes the final uncertainty in the outputs y [36]. Like with the CV value, which directly allows for comparison of the model's output accuracy, the G-criterion also gives an intuitive measure

Fig. 6 Flowchart of the MBDoE algorithm for adsorption isotherms and initialization based on Pankajakshan et al. [29]. Initialization comprises determining isotherm models, temperatures, and parameter bounds. The algorithm loops isotherm fits, statistic evaluation, finding the new measurement point $p_{\rm rel}^*$, and measuring at that pressure

for the accuracy of the chosen model-based design. This translation—from parameter uncertainty to output uncertainty—is achieved in a similar fashion to Gaussian error propagation [37]: The parameter covariance matrix V_{θ} is multiplied with the sensitivity of the outputs y with regard to the parameters θ , which are listed in the sensitivity matrix Q (cf. Eq. (12)) [38]. Thus, we find the uncertainty of the outputs u_y by multiplying the uncertainty of the parameters u_{θ} with the differentials $\partial y/\partial \theta$. Since we are interested in minimizing the deviation of the output of the isotherm models—the loading X—we choose the G-criterion with sensitivity matrix Q from Eq. (12) and parameter covariance matrix V_{θ} from Eq. (11):

$$\psi_{G} = \min \sum_{i}^{n_{y}} \sum_{j}^{n_{y}} Q V_{\theta} Q^{T}.$$
(21)

The resulting MBDoE process is shown as a flowchart in Fig. 6: The first step of the initialization of the MBDoE algorithm is the preselection of the isotherm models (here: Sips, DA, and BET), the parameter bounds (Table 8 in the SI), and the isotherm temperatures (given by the works of Young et al. [30] and Nguyen et al. [31]). In principle, the isotherm temperatures could be optimized simultaneously with the pressure creating a second design variable for the model-based design. Here, we decided against the temperature as a second design variable since the equilibration time for the temperature is quite large. Changing the temperature after each measurement would increase the overall measurement duration considerably compared to equilibrating only the pressure. Temperature-dependent isotherm parameters are only considered after the measurement of the first





Adsorption (2025) 31:103 Page 11 of 17 103

isotherm temperature is completed. The next step of the initialization are initial measurements. We decided on 3 initial measurements as the models have at least 3 parameters when temperature dependency is not considered. We set the initial measurements to the minimum, center, and maximum value of the design space. Note the maximum relative pressure, our gravimetric system was able to handle for water, was at $p_{\rm rel} = 0.85 \, {\rm g \, g^{-1}}$, $D = \{0, 0.85\}$.

Once the initial 3 measurements have been completed, all isotherm models are calibrated to the data. The measurement at $p_{\rm rel} = 0 \, \text{PaPa}^{-1}$ can be set to $X = 0 \, \text{g g}^{-1}$ since all isotherm models have to pass through the origin. If any of the models passed the χ^2 - and t-tests, the next predetermined temperature would be chosen. As none of the tests were usually passed after the initial measurements, a new measurement point $p_{\rm rel}^*$ is determined: Based on the calibrated isotherm models, the minimization problem of a joint MBDoE with the HR- and G-criterion (Eq. (22)) is solved: A numeric gradient-based solver from the Python package scipy minimizes the design criterion (i.e., the sum of normalized HR- and G-criterion from Eq. (22)) with respect to the pressure p. Since the HR-criterion identifies the minimum distance between all models and we are interested in the maximum distance, the HR-criterion gets a negative sign. In future studies, the effect of both G-and HR-criterion could also be weighted depending on the desired experimental design.

$$\varphi^* = \underset{\varphi \text{ in } D}{\operatorname{argmin}} \left\{ \frac{\psi_{G}}{\psi_{G, \text{ max}}} - \frac{\psi_{HR}}{\psi_{HR, \text{ max}}} \right\}. \tag{22}$$

The minimum of the design criterion corresponds to the next measurement point with the highest information content, thereby identifying the pressure at which to measure next. Afterwards, the gravimetric system measures at the new measurement point $p_{\rm rel}^*$ and the isotherm models are recalibrated using all data points. This cycle is repeated until any of the models satisfies the χ^2 - and t-test with a significance level of $\alpha=0.05$. Since the χ^2 -test relates model prediction error to uncertainty of the measurement, a value for the uncertainty of the gravimetric suspension balance is required. A maximal estimate of the uncertainty of our magnetic suspension balance $(u_X=0.0202\,\mathrm{g\,g^{-1}})$ is calculated in Appendix A and was used as a constant value throughout the measurements.

Once the statistical tests are satisfied, the next temperature is chosen and an initial measurement at the center of

the design space is set at $p_{\rm rel}^* = 0.5 \, {\rm Pa \, Pa}^{-1}$. As soon as

multiple temperatures are considered, the isotherm models automatically consider temperature-dependent parameters

as well. The calibration step of the isotherm models to the experimental data alters all parameters (temperature-dependent and -independent). Once the statistical tests of the last temperature are satisfied, the algorithm stops and returns the most probable model with its parameters.

4 Optimal experimental designs

4.1 Optimal design of a Type I isotherm

The detailed progression of the experimental design in Fig. 7 shows the Type I isotherm of Lewatit VP OC 1065/CO₂ for the temperatures 25/75/100 °C. The algorithm stopped after 8 measurements: 4 at 25 °C, 3 at 75 °C, and 1 at 100 °C. The algorithm correctly identified the Type I isotherm behavior for the first temperature after 4 data points and calibrated the Sips, DA, and BET models accordingly (Fig. 7 (a.6)).

The initial measurements at $p=0,\,0.5,\,$ and 1 bar and the initial model fits are shown in Fig. 7 (a.1). For the $\rm CO_2$ isotherm, the value of $p_{\rm max}=1\,{\rm bar}$ is chosen instead of $p_{\rm rel,\,max}=0.85\,{\rm Pa}\,{\rm Pa}^{-1}$ because the gravimetric system is not limited by condensation for the non-condensing gas. The models deviate the most around $p=0.08\,{\rm bar}$. The solver finds the optimum at $p=0.08\,{\rm bar}$ (dashed line in Fig. 7 (b.1)) and the next measurement is scheduled accordingly. After recalibrating the isotherm models, all models now show the Type I isotherm behavior (Fig. 7 (a.2)). At this point, the Sips model passes the χ^2 - and t-test, so the temperature switches to the next value at 75 °C.

According to the flowchart of the algorithm in Fig. 6, the first measurement at a new temperature is always at $p=0.5\,\mathrm{bar}$. Thus, the objective function is not evaluated in Fig. 7 (b.2) and (b.5) and instead the new design point is set to $p=0.5\,\mathrm{bar}$.

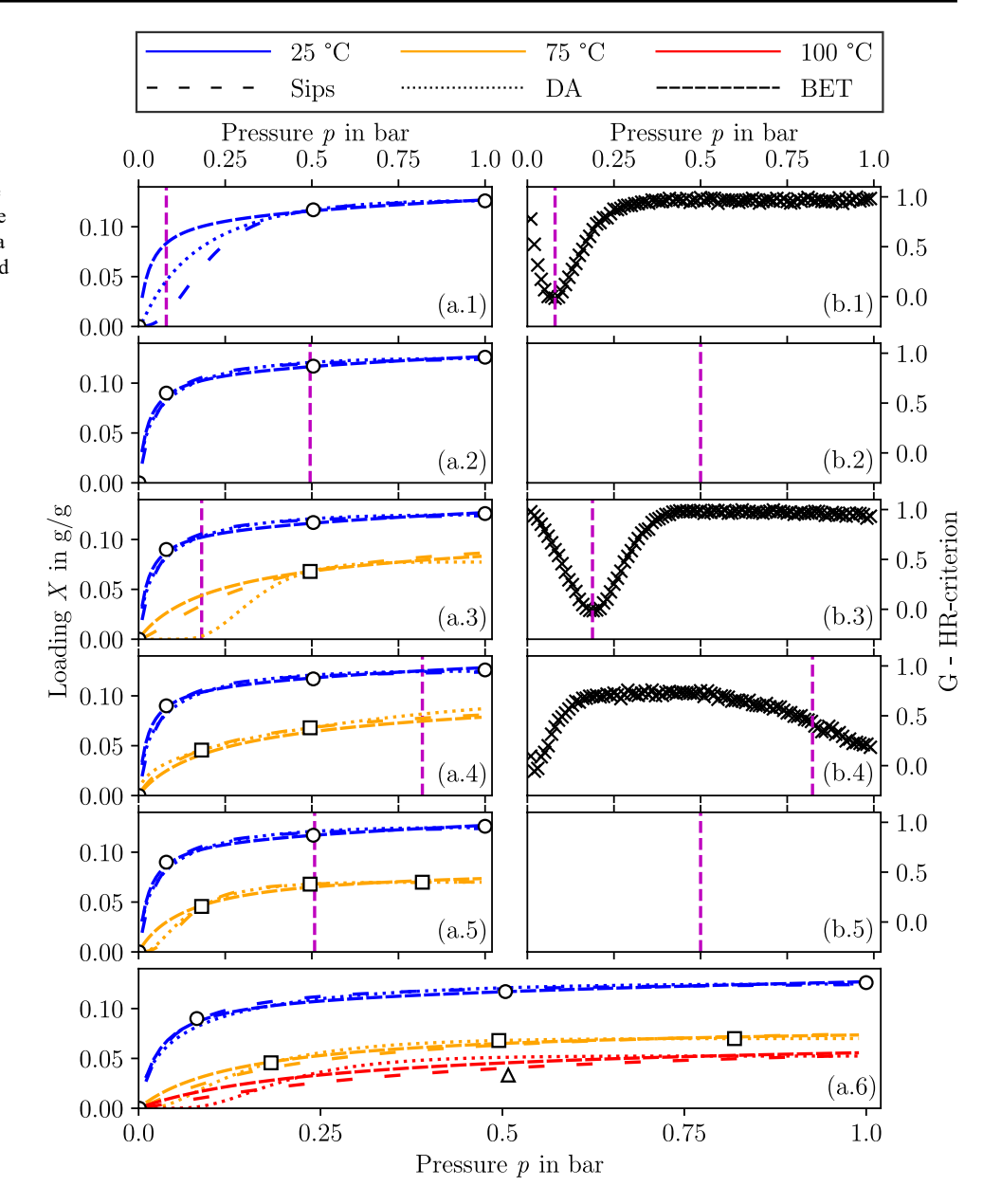
After recalibrating the models again, the 75 °C isotherms show the largest deviation at $p=0.18\,\mathrm{bar}$ (Fig. 7 (b.4)). The solver finds this optimum for model discrimination and a measurement at 0.18 bar is conducted. Since none of the models satisfies both the χ^2 - and t-test, the algorithm suggests to measure again at $p=0.85\,\mathrm{bar}$ (Fig. 7 (b.3)). The objective function is higher at this point than at the low relative pressure region, since the solver found a local optimum at the bound of the design space. Future implementations of the algorithm should implement a solver to find the global optimum. After the measurement, the Sips model again satisfies the statistical tests.

According to the MBDoE process from Fig. 6, the next and final measurement at the third temperature $T=100\,^{\circ}\mathrm{C}$ is conducted at $p=0.5\,\mathrm{bar}$. Alternatively to setting the initial measurement of every new temperature at $p=0.5\,\mathrm{bar}$,



103 Page 12 of 17 Adsorption (2025) 31:103

Fig. 7 Experimental design for a Type I isotherm with Lewatit VP OC 1065/CO₂. The left column (a.1)-(a.6) shows the measurement points for 25 °C (circles), 75 °C (squares), and 100 °C (triangles) and the fitted models. The right column (b.1)-(b.5) shows the objective function and the minima found by the solver (purple dashed lines)



this measurement could also have been chosen by optimal design: Since an estimate of the temperature-dependent isotherms is calibrated after the second isothermal temperature, every starting measurement for additional isothermal temperatures could be chosen based on the calibrated models instead of the fixed value of 0.5 bar. The automatic selection of a new starting value could be added to the algorithm in the future, improving the optimal experimental designs when many isotherms of the same adsorption pair are investigated.

After the first measurement at the last temperature, the Sips model passes the statistical tests. Since the Sips model is the only model to pass the tests, it is chosen although BET and DA model could potentially pass the tests if more measurements were conducted. This fact is also reflected in

the probabilities of the models, which are still in the same order of magnitude ($\Pr_{\rm Sips}=36.2\,\%,\,\Pr_{\rm DA}=35.5\,\%$, and $\Pr_{\rm BET}=28.3\,\%$).

The Sips model, which was only parametrized using 8 MBDoE measurements, is compared to the best reference model (BET isotherm) from Sect. 2.4 in Fig. 8. The Sips model from the MBDoE algorithm underestimates the loading of the $\rm CO_2$ isotherm for low pressures up to $p=0.1\,\rm bar$ for all temperatures, but matches the experimental data quite well for higher pressures (Fig. 8a). The best reference model was the BET model with a CV-value of 5.4% (Fig. 8b). The CV-value between the Sips model and the reference measurements is only 2.3 percentage points worse than the reference CV-value of the BET model. This result is very promising, as the Sips model was only



Adsorption (2025) 31:103 Page 13 of 17 103

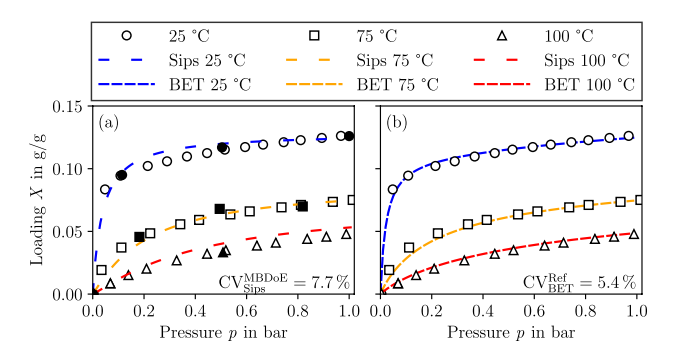


Fig. 8 Model fits for the Type I isotherm with Lewatit VPOC $1065/\mathrm{CO}_2$. The left figure (a) shows the fitted Sips model, which was determined as the most likely candidate by the MBDoE algorithm (filled points), and all reference data points (empty points). The right figure (b) shows the reference BET model with the highest probability and lowest CV-value as well as all data points. An analysis of the measurement uncertainty is given in the SI

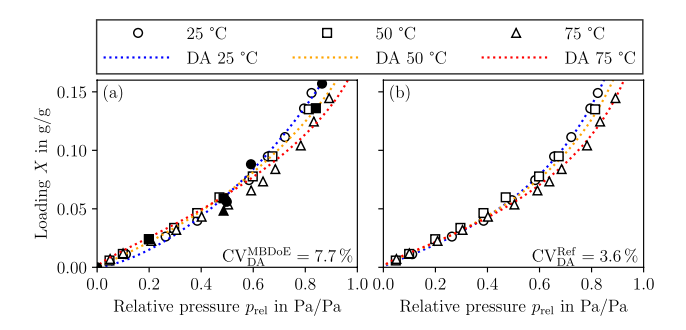


Fig. 9 Resulting model fits for the Type III isotherm with Lewatit VP OC 1065/H₂O. The left figure (a) shows the fitted DA model, which was determined as the most likely candidate by the MBDoE algorithm (filled points), and all reference data points (empty points). The right figure (b) shows the reference DA model with the highest probability and lowest CV-value as well as all data points. An analysis of the measurement uncertainty is given in the SI

calibrated using 8 measurements (filled data points in Fig. 8) and the reference model was calibrated using 36 data points (empty data points). This way, we were able to save 78% of the experimental effort while still achieving a reasonably accurate model with a value of $\mathrm{CV^{MBDoE}} = 7.7\%$ compared to $\mathrm{CV^{Ref}} = 5.4\%$.

4.2 Optimal design of a Type III isotherm

The same algorithm is repeated for the adsorption pair Lewatit VP OC $1065/\mathrm{H}_2\mathrm{O}$ (Type III isotherm) and the temperatures 25/50/75 °C. The detailed progression of the MBDoE experiments is shown in Figure 13. The algorithm stops after 9 data points: 4 at 25 °C, 4 at 50 °C and 1 at 75 °C. The DA-model is selected as in the reference measurement.

The isotherm Type III is not identified until 7 measurements are conducted as the isotherm type is more ambiguous for this adsorption pair. When looking closely

at the reference measurement in Fig. 4, a small plateau between $p_{\rm rel}=0.1\,{\rm Pa\,Pa^{-2}}-0.2\,{\rm Pa\,Pa^{-2}}$ can be seen. We believe that this plateau is caused by a physical effect where classical adsorption switches to pore condensation. The isotherm type of Lewatit VP OC $1065/{\rm H_2O}$ would therefore in fact be Type II instead of Type III. This ambiguity is the reason the isotherm type is identified later than the Type I isotherm from the last section. Even the final model reflects the Type II isotherm behavior for higher isotherm temperatures (Fig. 9). This result shows that the MBDoE algorithm identified a possible misconception by us as experimenters assuming a Type III isotherm behavior, when in fact the adsorption pair could also be a Type II isotherm.

In contrast to the Type I isotherm, the solver finds a local optimum for measurement number 6 instead of the better optimum at high relative pressure (Figure 13 in the SI). Interestingly, the missed optimum at high relative pressure is measured with the next data point leading to only minimal deviation from the global optimal experimental design.

The calibrated model from the MBDoE process is compared to the best reference model in Fig.9. This time, the MBDoE algorithm identified the DA model, which was also determined as the most accurate model through fitting of the reference data. Although the DA model from our MBDoE process was only calibrated using 9 measurements, it provides a CV-value of 7.7% towards the original reference data. The remaining offset to the reference DA model is mainly the isotherm curve below $p_{\rm rel}=0.5$.

The temperature dependency of the isotherms is overestimated between $0 < p_{\rm rel} < 0.4\,{\rm Pa\,Pa^{-1}}$ in Fig. 9 (left), trying to match more of the Type II isotherm behavior. This result points out a challenge for the MBDoE algorithm: We try to calibrate a temperature-dependent model to a predominantly temperature-insensitive region. A simpler isotherm model might provide better results here. The result for the Type II/III isotherm is nonetheless also quite promising as we increase the CV-value by only 4.1 percentage points compared to the reference ${\rm CV^{Ref}}.$ We therefore save 70% of the experimental effort while still providing a reasonably accurate model.

4.3 Optimal design of a Type V isotherm

Finally, the MBDoE algorithm is applied to the Type V isotherm of the adsorption pair BAM-P109/H₂O for the temperatures 25/50/80 °C. The detailed MBDoE experiments are shown in Figure 14. For the Type V isotherm, the algorithm stops after 9 measurements: 5 at 25 °C, 3 at 50 °C, and 1 at 80 °C. The correct isotherm shape is identified after 3 measurements. The solver gets caught at the measurement boundary for the first experiment, but finds the missed global optimum at the very next iteration. The BET model



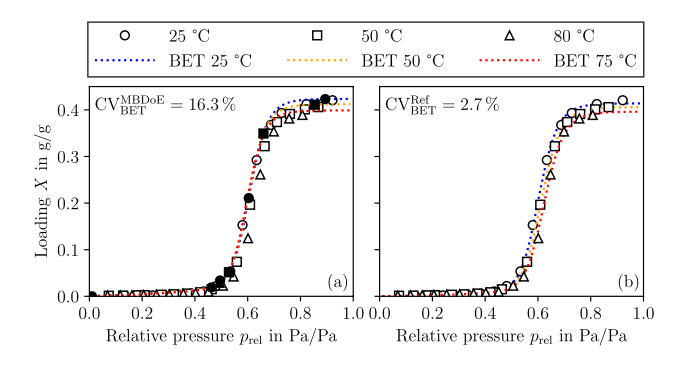


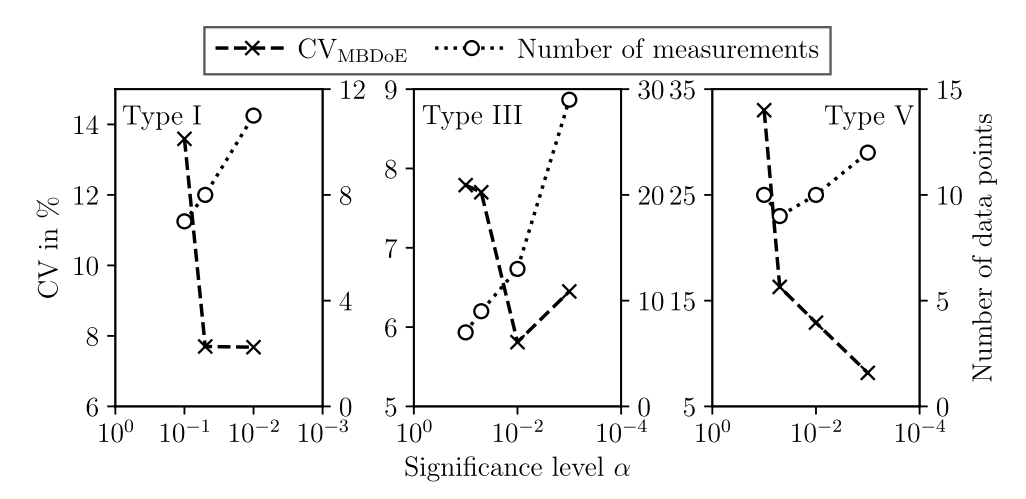
Fig. 10 Resulting model fits for the Type V isotherm with BAM-P109/ $\rm H_2O$. The left figure (a) shows the fitted BET model, which was determined as the most likely candidate by the MBDoE algorithm (filled points), and all reference data points (empty points). The right figure (b) shows the reference BET model with the highest probability and lowest CV-value as well as all data points. An analysis of the measurement uncertainty is given in the SI

is selected by the MBDoE algorithm with a probability of $\mathrm{Pr}_{\mathrm{BET}}=59\,\%.$ The low probability indicates that a second model (Sips in this case) matches the measurement data reasonably well. The BET model was also the reference model with the lowest CV-value from Sect. 2.4, so, the correct model is chosen despite the low absolute probability value.

Both the BET model from optimal design and from the reference measurements are compared in Fig. 10. The BET model parametrized by the MBDoE algorithm matches the 25 °C isotherm very well. However, the 50 °C and 80 °C isotherm are not described perfectly as the temperature jump of the S-shaped isotherm should move to higher relative pressure for higher isotherm temperatures. The fit could be improved by weighing the temperature-dependent parameters more within the objective function of the parameter precision.

Since the offset occurs in the steepest region of the curve, the CV-value becomes quite large ($\rm CV^{MBDoE}=16.3\,\%$) as it only considers measurement error in y-direction. Nonetheless, a reasonable isotherm model is parametrized by the

Fig. 11 Sensitivity analysis of the stopping criterion for MBDoE of adsorption isotherms of Type I (left), Type III (center), and Type V (right). The CV-values and the number of experimental points are shown over the significance level α of both χ^2 - and t-test



MBDoE algorithm with only 9 measurements compared to 48 data points of the reference measurement saving 81% of the data points.

4.4 Sensitivity analysis of the stopping criterion

From the results of the last section, we can see that the MBDoE algorithm works, the correct isotherm Types are identified, and the experimental effort is reduced by 70-81%. The isotherm models are parametrized quite well; however, measuring a few more points could potentially improve parameter estimation. Furthermore, passing the statistical tests is highly dependent on the loading measurement uncertainty of the device: A high measurement uncertainty leads to the isotherm models passing the statistical test with less measurement points, as more model uncertainty is tolerated. The trade-off between model accuracy and experimental effort is analyzed in this section. Since, the experiments are quite time consuming, this analysis is performed in-silico with the parametrized isotherm models from Sect. 2.4 and the measurement uncertainty of the gravimetric system from the SI.

The trade-off between model accuracy and experimental effort can be adjusted by adapting the significance level α . So far, the significance level was set to 0.05, leading to termination of the MBDoE algorithm after 8-9 measurements. When decreasing the significance level further, the statistical tests terminate the algorithm later, as higher requirements are set to model lack-of-fit (χ^2 -test) and parameter precision (t-test). The expectation of a lower significance level would be to reduce the CV-value of the isotherm models, although with more data points.

The trade-off between the number of measurements and the achieved CV-value of the isotherm models parametrized by the MBDoE algorithm shows that the CV-value decreases for a decreasing significance level, however, not beyond a threshold of 7.7% for the Type I isotherm (Fig. 11 (left)). Also, at no point, the BET model is chosen as the most



Adsorption (2025) 31:103 Page 15 of 17 103

probable model due to a local minimum of the parameter estimation for the BET model. If the correct minimum for the optimal BET parameters is never found, the Sips model remains the best model, limiting the CV-value to 7.7% even with more data points. Switching the solver for the automatic curve fit from a local solver to a global algorithm could solve this issue in the future.

For the Type III isotherm, decreasing the significance level from 0.05 to 0.01 increases the number of measurements from 9 to 13 while also decreasing the CV-value from 7.7 to 5.8% (Fig. 11 (center)). Decreasing the significance level to 0.001 leads to a large increase of measurement points up to 29 points. However, this increase does not benefit the CV-value, pointing again towards possible improvements to the automatic curve fit. With 29 instead of 30 data points, the same model fit as the reference model should be possible.

Lastly, the CV-value can be further decreased from 16.3 to 8.2% for the Type V isotherm by adjusting the significance level (Fig. 11 (right)). Surprisingly, the number of data points only increases slightly from 9 to 12 points, which would be the preferred option as three more points decrease the CV-value by half.

The results show that a lower significance level α can lead to better isotherm models, when the automatic isotherm calibration identifies the global minimum of the isotherm parameters. Otherwise, the second best isotherm model is chosen and a lower significance level does not improve model accuracy, in case the second-best model is already optimally parametrized. Furthermore, decreasing the significance level to 0.01 or 0.001 can be sensible depending on the uncertainty of the loading: 3 to 4 more data points decreased the CV-value between 1.9 and 8.1 percentage points. On the other hand, if the significance level is too low and the choice of isotherm models is poor, the algorithm may fail to converge. In practice, the set of isotherms should be expanded and the significance level adjusted to the measurement error should convergence issues arise.

Overall, if isotherm data is available from other sources, we advise to perform an *in-silico* MBDoE analysis of the literature data prior to application of the MBDoE algorithm to the experiment. This way, the dependence of the statistical tests on the measurement uncertainty can be estimated.

5 Conclusion

In chemical engineering, the framework of model-based design of experiments (MBDoE) is state of the art to reduce experimental effort when calibrating models. For the field of adsorption, equilibrium measurements are quite tedious, however, accurate isotherm models are essential to design

adsorption processes. To the best of our knowledge, we combined the two research fields for the first time "live" and developed an open-source iterative MBDoE algorithm for adsorption isotherm measurements. This way, we reduce the experimental effort of adsorption equilibrium measurements while maintaining high isotherm model accuracy. The MBDoE algorithm updates the isotherm models after each measurement and plans the next measurement point based on the parametrized isotherm models. The algorithm is based on MBDoE choosing an experimental point, which jointly improves model discrimination and parameter precision at the same time (j-MBDoE). The process stops after at least one isotherm model satisfies the χ^2 - and t-test. In the end, the most probable isotherm model is returned. Our analysis leads to the following 4 main conclusion:

First, the number of measurements can be reduced by 70-81% when parametrizing an isotherm model with temperature-dependent parameters for a set of three isotherm temperatures. This reduction can be achieved without a-priori knowledge of the most suitable isotherm model or its parameters. The measurement points equilibrate slower than the conventional approach of equidistant adsorption isotherms, since the changes in relative pressure are larger for the MBDoE approach. The benefit of using the MBDoE approach thus increases for more isotherms of the same working pair, since fewer measurement points are needed compared to the conventional approach. The correct model (according to our reference measurements) was chosen by the MBDoE algorithm for 2 of 3 isotherm types, while the second-best model is chosen for the last isotherm type. The model accuracy decreased between 2.3 and 13.6 percentage points in CV-value, which is quite promising, considering the large savings in experimental time.

Second, the MBDoE algorithm was able to identify the isotherm type by itself and scheduled measurements to determine whether the adsorption pair Lewatit VP OC 1065/H $_2$ O was in fact a Type II or Type III isotherm. The reference measurement shows a small plateau between $p_{\rm rel}=0.1\,{\rm Pa}\,{\rm Pa}^{-1}$ and $0.2\,{\rm Pa}\,{\rm Pa}^{-1},$ which we initially ignored and calibrated a Type III isotherm model. However, the MBDoE algorithm identified the potential mismatch and calibrated an isotherm model devoid of our bias of the experimenters.

Third, the significance level α of the statistical tests can be adjusted to match the measurement uncertainty in the employed experimental setup. We showed in a sensitivity analysis that 3-4 more isotherm points during the design of experiments can up to halve the CV-value. This way, each experimenter can individually set the desired trade-off between experimental effort and model accuracy by adjusting the significance level according to a prior sensitivity analysis.



Fourth, automatic isotherm calibration to the experimental data is crucial for the success of the MBDoE algorithm. Sound parameter bounds have to be set and a potent solver should be employed. If the isotherm models are not calibrated with high accuracy, the ensuing experimental design cannot achieve its full potential as its then based on inaccurate isotherm models.

These findings show the potential of measuring adsorption isotherms on the basis of model-based design of experiments instead of measuring equidistantly, highlighting a large potential to save experimental effort while maintaining high model accuracy.

Supplementary Information The online version contains supplementary material available at https://doi.org/10.1007/s10450-0 25-00653-0.

Acknowledgements We thank Jan Seiler, Xiaoxian Yang, and Mijndert van der Spek for fruitful discussions as well as Fabian Spinrath and Florian Seibel for assisting with programming. We further thank Can Kececi, Thomas Petrzik, and Lukas Stempfle for their experimental work in the lab. This work has been published as part of the dissertation of Matthias Henninger by the University Library of RWTH Aachen University under the following link: https://doi.org/10.1815 4/RWTH-2025-01170.

Author Contributions Matthias Henninger: Conceptualization, Methodology, Validation, Formal analysis, Investigation, Resources, Visualization, Writing—Original Draft. Patrik Postweiler: Methodology, Writing—Review & Editing. Mirko Engelpracht: Conceptualization, Writing—Review & Editing. Federico Galvanin: Methodology, Formal analysis, Writing—Review & Editing. André Bardow: Conceptualization, Methodology, Writing - Review & Editing, Supervision, Funding acquisition.

Funding The authors acknowledge funding by the German Research Foundation (DFG), "Major Instrumentation Initiatives", project number: 410205678.

Matthias Henninger acknowledges funding by the NRW Federal Ministry of Economy, Innovation, Digitization, and Energy, "progres. nrw – Research", project number: 005-2302-0007_0365 and by the RWTH Aachen University and the German Academic Exchange Service (DAAD): "ERASMUS+ – Staff mobility program" and would like to thank the UCL Department of Chemical Engineering for hosting the ERASMUS+ mobility.

Data Availability The measurement data for reference and MBDoE measurements from Figure 3 to Figure 5 and Figure 7 to Figure 10 are available in the supplementary information of this article. The python package "Model-Based Design of Adsorption Experiments" (MBDoAE) to measure the iterative MBDoE adsorption isotherm is also available in the supplementary information of this article.

Declarations

Competing interests The authors declare no competing interests.

Open Access This article is licensed under a Creative Commons Attribution 4.0 International License, which permits use, sharing, adaptation, distribution and reproduction in any medium or format, as long as you give appropriate credit to the original author(s) and the

source, provide a link to the Creative Commons licence, and indicate if changes were made. The images or other third party material in this article are included in the article's Creative Commons licence, unless indicated otherwise in a credit line to the material. If material is not included in the article's Creative Commons licence and your intended use is not permitted by statutory regulation or exceeds the permitted use, you will need to obtain permission directly from the copyright holder. To view a copy of this licence, visit http://creativecommons.org/licenses/by/4.0/.

References

- Rother, J., Fieback, T.: Multicomponent adsorption measurements on activated carbon, zeolite molecular sieve and metalorganic framework. Adsorption 19(5), 1065–1074 (2013)
- Keller, J.U.: Gas Adsorption Equilibria: Experimental Methods and Adsorptive Isotherms. Microsystems. Springer, New York (2005)
- Franceschini, G., Macchietto, S.: Model-based design of experiments for parameter precision: state of the art. Chem. Eng. Sci. 63(19), 4846–4872 (2008)
- Galvanin, F., Cao, E., Al-Rifai, N., Gavriilidis, A., Dua, V.: A joint model-based experimental design approach for the identification of kinetic models in continuous flow laboratory reactors. Comput. Chem. Eng. 95, 202–215 (2016)
- Box, G.E.P., Lucas, H.L.: Design of experiments in non-linear situations. Biometrika 46, 77–90 (1959)
- Atkinson, A.C., Bogacka, B., Bogacki, M.B.: D- and t-optimum designs for the kinetics of a reversible chemical reaction. Chemom. Intell. Lab. Syst. 43(1-2), 185-198 (1998)
- Rodríguez-Aragón, L.J., López-Fidalgo, J.: Optimal designs for the arrhenius equation. Chemom. Intell. Lab. Syst. 77(1–2), 131– 138 (2005)
- Rodríguez-Aragón, L.J., López-Fidalgo, J.: T-, d- and c-optimum designs for bet and gab adsorption isotherms. Chemom. Intell. Lab. Syst. 89(1), 36–44 (2007)
- Mannarswamy, A., Munson-McGee, S.H., Steiner, R., Andersen, P.K.: D-optimal experimental designs for freundlich and langmuir adsorption isotherms. Chemom. Intell. Lab. Syst. 97(2), 146–151 (2009)
- Munson-McGee, S.H., Mannarswamy, A., Andersen, P.K.: Designing experiments to differentiate between adsorption isotherms using t-optimal designs. J. Food Eng. 101(4), 386–393 (2010)
- Munson-McGee, S.H., Mannarswamy, A., Andersen, P.K.: D-optimal designs for sorption kinetic experiments: slabs. J. Food Eng. 104(3), 461–466 (2011)
- Munson-McGee, S.H., Mannarswamy, A., Andersen, P.K.: D-optimal designs for sorption kinetic experiments: cylinders. J. Food Eng. 104(2), 202–207 (2011)
- Munson-McGee, S.H.: Dimensionless analysis of d-optimal designs for 1-dimensional sorption kinetic experiments. Sep. Sci. Technol. 49(18), 2856–2862 (2014)
- Paquet-Durand, O., Zettel, V., Hitzmann, B.: Optimal experimental design for parameter estimation of the peleg model. Chemom. Intell. Lab. Syst. 140, 36–42 (2015)
- Kalyanaraman, J., Kawajiri, Y., Realff, M.J.: Bayesian design of experiments for adsorption isotherm modeling. Comput. Chem. Eng. 135, 106774 (2020)
- Kober, R., Schwaab, M., Steffani, E., Barbosa-Coutinho, E., Pinto, J.C., Alberton, A.L.: D-optimal experimental designs for precise parameter estimation of adsorption equilibrium models. Chemom. Intell. Lab. Syst. 192, 103823 (2019)



Adsorption (2025) 31:103 Page 17 of 17 103

 Kober, R., Schwaab, M., Steffani, E., Barbosa-Coutinho, E., Pinto, J.C.: D-optimal experimental designs for precise parameter estimation of adsorption equilibrium models: initial concentration and solvent volume to adsorbent mass ratio as independent variables. Adsorption 27(7), 1013–1022 (2021)

- Postweiler, P., Gibelhaus, A., Engelpracht, M., Seiler, J., Bardow, A.: Experimental validation of a dynamic adsorption chiller model using optimal experimental design. In: ISHPC 2021 proceedings, pp. 28–32 (2021)
- 19. Ward, A., Pini, R.: Integrated uncertainty quantification and sensitivity analysis of single-component dynamic column breakthrough experiments. Adsorption **28**(3–4), 161–183 (2022)
- Toffoli de Oliveira, J., Da Luz Arsufi, A.B., Estumano, D.C., Féris, L.A.: Bayesian computational technique for modeling caffeine adsorption in a fixed-bed column: Use of the maximum adsorption capacity deterministically and experimental design. Ind. Eng. Chem. Res. 62(18), 7127–7137 (2023)
- Gast, T.: Waagen mit freischwebender magnetischer aufhängung (in german). Naturwissenschaften 56(9), 434–438 (1969)
- Lösch, H.W., Kleinrahm, R., Wagner, W.: Neue magnetschwebewaagen für gravimetrische messungen in der verfahrenstechnik (in german). Chem. Ing. Tec. 66(8), 1055–1058 (1994)
- Dresp, G.: Development of an optical-gravimetric system for determination of swellling-corrected sorption behavior and mass transfer characteristics of liquid sorbents in forced flow through atmospheres. PhD thesis, Ruhr-University Bochum, Bochum (2018)
- 24. Sips, R.: On the structure of a catalyst surface. J. Chem. Phys. **16**(5), 490–495 (1948)
- 25. Brunauer, S., Deming, L.S., Deming, W.E., Teller, E.: On a theory of the van der waals adsorption of gases. J. Am. Chem. Soc. **62**(7), 1723–1732 (1940)
- Aristov, Y.I.: Applying the potential theory of adsorption for adsorptive heat transformation. Adsorption 29, 225–235 (2023)
- Do, D.D.: Adsorption analysis: Equilibria and kinetics. Series on chemical engineering. Imperial College Press, London (1998)
- Shimizu, S., Matubayasi, N.: Temperature dependence of sorption. Langmuir 37(37), 11008–11017 (2021)
- Pankajakshan, A., Bawa, S.G., Gavriilidis, A., Galvanin, F.: Autonomous kinetic model identification using optimal experimental design and retrospective data analysis: methane complete oxidation as a case study. React. Chem. Eng. 8, 3000–3017 (2023)
- Young, J., García-Díez, E., Garcia, S., van der Spek, M.: The impact of binary water-co2 isotherm models on the optimal performance of sorbent-based direct air capture processes. Energy Environ. Sci. 14(10), 5377–5394 (2021)
- Nguyen, H.G.T., Toman, B., van Zee, R.D., Prinz, C., Thommes, M., Ahmad, R., Kiska, D., Salinger, J., Walton, I.M., Walton,

- K.S., Broom, D.P., Benham, M.J., Ansari, H., Pini, R., Petit, C., Adolphs, J., Schreiber, A., Shigeoka, T., Konishi, Y., Nakai, K., Henninger, M., Petrzik, T., Kececi, C., Martis, V., Paschke, T., Mangano, E., Brandani, S.: Reference isotherms for water vapor sorption on nanoporous carbon: results of an interlaboratory study. Adsorption **29**, 113–124 (2023)
- Song, A.-Y., Young, J., Wang, J., Fricke, S.N., Piscina, K., Giovine, R., Garcia, S., van der Spek, M., Reimer, J.A.: Discerning molecular-level co2 adsorption behavior in amine-modified sorbents within a controlled co2/h2o environment towards direct air capture. J. Mater. Chem. A 12, 25875–25886 (2024)
- Buzzi-Ferraris, G., Forzatti, P., Paolo, C.: An improved version of a sequential design criterion for discriminating among rival multiresponse models. Chem. Eng. Sci. 45(2), 477–481 (1990)
- Donckels, B.M., De Pauw, D.J., De Baets, B., Maertens, J., Vanrolleghem, P.A.: An anticipatory approach to optimal experimental design for model discrimination. Chemom. Intell. Lab. Syst. 95(1), 53–63 (2009)
- Schwaab, M., Luiz Monteiro, J., Carlos Pinto, J.: Sequential experimental design for model discrimination: Taking into account the posterior covariance matrix of differences between model predictions. Chem. Eng. Sci. 63(9), 2408–2419 (2008)
- Cenci, F., Pankajakshan, A., Facco, P., Galvanin, F.: An exploratory model-based design of experiments approach to aid parameters identification and reduce model prediction uncertainty. Comput. Chem. Eng. 177, 108353 (2023)
- JCGM. Evaluation of measurement data: Guide to the expression of uncertainty in measurement (GUM series, 1. edition):
 JCGM100:2008. https://www.bipm.org/utils/common/document s/jcgm/JCGM 100 2008 E.pdf (2008). Accessed 18 July 2023
- Dechambre, D., Wolff, L., Pauls, C., Bardow, A.: Optimal experimental design for the characterization of liquid-liquid equilibria. Ind. Eng. Chem. Res. 53(50), 19620–19627 (2014)
- TLK Thermo GmbH. TILMedia Suite. https://www.tlk-thermo.com/index.php/en/software/tilmedia-suite (2023). Accessed 15 May 2024
- Yang, X., Kleinrahm, R., McLinden, M.O., Richter, M.: Uncertainty analysis of adsorption measurements using commercial gravimetric sorption analyzers with simultaneous density measurement based on a magnetic-suspension balance. Adsorption 26(4), 645–659 (2020)
- Bevington, P.R., Robinson, D.K.: Data Reduction and Error Analysis, 3rd edn. McGraw-Hill, New York (2003)

Publisher's Note Springer Nature remains neutral with regard to jurisdictional claims in published maps and institutional affiliations.

